RSC Advances

ROYAL SOCIETY OF CHEMISTRY

www.rsc.org/advances

Adsorption of phosphate on surface of magnetic reed: characteristics, kinetic, isotherm, desorption, competitive adsorption and mechanistic studies

Tiantian Wang[a,b], Xing Xu[*a], Zhongfei Ren[a], Baoyu Gao[a], Hantao Wang[a]

[a]Shandong Key Laboratory of Water Pollution Control and Resource Reuse, School of Environmental Science and Engineering, Shandong University, Jinan 250100, PR China

[b]School of resource and environment, Huazhong Agricultural University, Wuhan, PR China

Abstract: A magnetic biocomposite was prepared by Fe_3O_4 in-situ co-precipitation and amine functionalization processes by using virgin reed as starting material. The characteristics of amine cross-linked magnetic reed (ACMR) as well as phosphate-loaded/regenerated ACMR were evaluated by using FTIR, TEM, SEM, VSM and XPS. Adsorption properties of ACMR for phosphate were also determined. Results indicated that the average particle diameter of present Fe_3O_4 in ACMR was approximately 10.4 nm. Analysis of XPS indicated that uptake of phosphate by ACMR was based on N+ in quaternary nitrogen N1s. The atomic ratio of Fe and N in regenerated ACMR was about 0.41% and 10.75%, which was a bit lower as compared with that in clean sample (0.46% and 11.02%); this indicated a small loss of Fe_3O_4 and amine groups on surface of ACMR during adsorption-desorption cycles. The calculated Q_{max} from Langmuir model were about 31.4-37.0 mg/g at 20-45 ℃, which has shown comparable phosphate uptake capacity by contrast with most reported work. In addition, competitive adsorption revealed that the inhibition effect was more significant for anions with greater tendency to undergo ion exchange reaction (e.g. sulfate, nitrate and chloride) with quaternary ammonium groups on ACMR.

Keywords: Reed; Adsorption; Magnetic biocomposite; Phosphate; XPS

1. Introduction

The presence of phosphate in wastewaters provides an additional nutrient in the near static water bodies. As a result, an excessive growth of photosynthetic aquatic micro- and macro-organisms is encouraged in such water bodies which ultimately become a major cause for the eutrophication of such receiving waters [1-3]. Therefore wastes containing phosphate must meet the discharge limits for phosphates as 0.5–1.0

*Corresponding author: Tel.: +86-531-88361912; Fax: +86-531-88364513
E-mail: xuxing@sdu.edu.cn

mg/l P. In order to meet effluent quality standards, the removal of phosphate from wastewaters prior to discharge into natural waters is required.

In wastewater-treatment technology, various techniques such as chemical precipitation, reverse osmosis, electrodialysis, contact filtration, adsorption and advanced biological methods have been successfully applied for phosphate removal[4, 5]. Adsorption is one of the techniques, which is comparatively more useful and economical for phosphate removal. Adsorption has been using as an alternative method for phosphate removal in wastewater treatment since 1960s. Due to intensified ‘‘green thinking’’ in process industry as well as environmental protection, the applications of low cost and easily available natural products in wastewater treatment have emerged as a viable option[6, 7]. These available materials included agricultural products and by-products, industrial by-products/wastes, hydrotalcites, soils and constituents, oxides and clay minerals, etc [2, 3, 5, 7].

Using the low-cost agricultural by-products as the effective adsorbents seems to be an acceptable access to uptake the phosphate from aqueous media. These agricultural by-products based bio-sorbents were prepared by impregnating with metal ions or amine groups which can catch phosphate by ligand/ion exchange mechanisms or activating with porous structures for adsorption of phosphate through pore adsorption [7-9]. However, conventional cellulose-based adsorbents are difficult to be recovered from wastewater except by filter or high speed centrifugation. The preparation of magnetic bio-sorbents would be a good alternative to solve this problem [9-12]. Compared to the reported bio-sorbents, a combination between bio-sorbents and iron oxide particles can pose an efficient biocomposite material, which could possibly show high adsorption capacity, intensified stability, and easy recovery from treated effluents by applying an external magnetic field. At present, there is only a few researches on the applications of these magnetic biomaterials, which mainly focus on the removal of dyes, Cr(VI) and heavy metal cations from liquids as well as enzyme immobilization [10-14]. Therefore, to explore a magnetic bio-sorbent with a large phosphate adsorption capacity has an important realistic meaning.

In this study, virgin reed was used as the starting material to prepare the magnetic biosorbent. Fe_3O_4 was first introduced onto the surface of virgin reed by the in-situ co-precipitation method [15, 16]. It was then modified with amine groups through grafting of epichlorohydrin, and ethanediamine followed by reaction with trimethylamine, forming the amine crosslinked magnetic reed (ACMR) [1-3, 17-19].

The resulting biocomposite materials well as phosphate laden sample was characterized by Fourier transform infrared spectroscopy (FTIR), transmission electron microscopy (TEM), Scanning Electron Microscope (SEM), vibrating sample magnetometer (VSM), X-ray photoelectron spectroscopy (XPS) and X-ray diffraction (XRD). Subsequently, the biocomposite material was used for the removal of phosphate from liquid by evaluating its adsorption capacities as a function of pH, concentration, contact time, temperature and reusability.

2. Methods and materials

2.1. Materials and reagents

The virgin reed was obtained from Weishan Lake in Shandong Province, China. It was first dried and then sieved to 1-4 mm before use. All reagents used in tests including $FeSO_4$, $FeCl_3$, NaH_2PO_4, epichlorohydrin, N,N-dimethylformamide, ethanediamine and trimethylamine were of analytically pure and were bought from Sinopharm Group Co. Ltd.

2.2. Preparation of ACMR

The preparation of amine crosslinked magnetic sample was conducted in a two-step reaction composed of (i) Fe_3O_4 in-situ co-precipitation, and (ii) amine functionalization process (Fig. 1).

(i) The Fe_3O_4 was first introduced onto the surface of virgin reed by the in-situ co-precipitation method based on hydrogen bond. In the co-precipitation process, virgin reed (4.0 g) was suspended in a 240 mL mixed solution with $FeSO_4$ of 0.125 mol/L and $FeCl_3$ of 0.25 mol/L. The reaction system was kept in an oxygen-free condition by purging with N_2. After adding 25 mL of $NH_3 \cdot H_2O$ (25%), the reaction temperature was raised to 70 °C and held for about 4 h. Then the Fe_3O_4 loaded reed was washed with deionized water and dried in a vacuum oven at 85 °C for 4 h.

(ii) Thereafter, 15 mL of epichlorohydrin and 10 mL of N,N-dimethylformamide were reacted with 6.0 g of magnetic reed and the mixture was stirred for 1 h at 85 °C. Ethanediamine (5 mL) was then added dropwise into the system and stirred for 30 min, followed by adding 10 ml of trimethylamine (stirred for 1 h at 85 °C). The primary products were washed with deionized water and dried for 12 h at 80 °C. The final samples (ACMR) were then collected and stored for use (ACMR with 19.6 g was obtained).

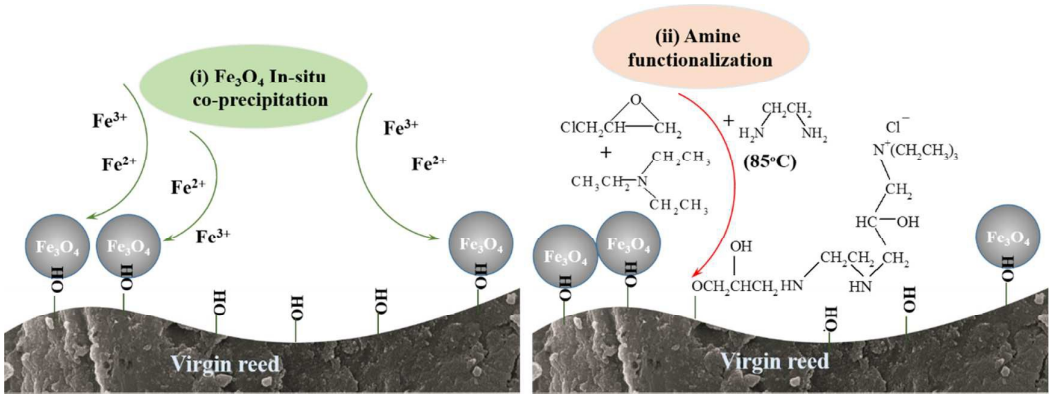

Fig. 1. Preparation steps for amine crosslinked magnetic reed

2.3. Characteristics of all magnetic samples

The magnetic properties of the biocomposite material (ACMR), phosphate laden ACMR and regenerated ACMR were measured as VSM by magnetometer (LDJ9500) at room temperature. Scanning electron microscopy (SEM) images and Transmission electron microscopy (TEM) of ACMR were obtained with NoVa™ Nano SEM 250and FEI Tecnai G20, respectively.

The functional groups in ACMR and phosphate laden ACMR as well as phosphate solid were evaluated by using the FTIR technique (Perkin-Elmer ‘‘Spectrum BX’’ spectrometer) with spectrums canned from 400 to 4000 cm^{-1}.

The textural structure including BET surface area, pore volume and pore size was determined by nitrogen adsorption/desorption isotherms at 196 C according to the Brunauer–Emmett–Teller (BET) principle (JW-BK122W, Beijing JWGB Sci. & Tech. Co., Ltd., China).

The surface binding state and elemental speciation of ACMR, phosphate laden ACMR and regenerated ACMR were analyzed by XPS. The measurements were performed by a spectrometer (ESCALAB 250) with Mg*K*α irradiation (1486.71 eV of photons) as X-ray source. The phosphate laden ACMR was prepared by mixing 0.1 g of ACMR with 50 ml of phosphate solution (1000 mg/L) for 12 h.

XRD patterns of powdered ACMR samples were carried out using a Rigaku D/MAX-YA diffractometer with Cu-Kα radiation at a voltage of 40 kV and a current of 40 mA ,employing a scanning speed of 0.5 s per step in the range of diffracting angles 2θ from 10^{o} to 70^{o}.

2.4. Adsorption tests

In the pH effect experiment, the initial pH of phosphate solution (40 mg P/L) was first adjusted to pH range from 3.4 to 10.8 by 1 mol/L of HCl/NaOH solutions.

Thereafter, 0.1 g ACMR was added to 25 ml of respective solutions in 100 ml Erlenmeyer flasks. Mixing was carried out at room temperature (20±1°C) on a rotary mixer and then the residual phosphate was determined at the wavelengths of UV-maximum (λ_{max}) at 700 nm by ammonium molybdate spectrophotometric method through a UV–visible spectrophotometer (model UV754GD, Shanghai).

Isotherm experiments was carried out by maintaining the water bath at 20, 35 and 45°C. ACMR(0.1 g) were added to a set of 100 ml Erlenmeyer flasks containing 25 mL of phosphate solutions (pH: 6.0~7.0) with concentrations range of 25-500 mg P/L. After mixing for 6 h, the residual phosphate was then detected.

Adsorption kinetics experiments were carried out by mixing a series of ACMR (0.1 g) with 25 ml of phosphate solutions with concentrations of 10, 20 and 40 mg P/L (20±1°C). Each samples were extracted at required time intervals and then were filtered to analyze the residual phosphate concentrations in solutions.

The spent ACMR was mixed with NaCl, NaOH or HCl solution (0.1 mol/L) for 6 h. After washed with distilled water for three times, the regenerated ACMR were used again in the subsequent experiments. The adsorption-desorption tests were conducted for 4 cycles and each regeneration efficiency was evaluated.

The competitive adsorption tests were evaluated by mixing the individual anions (e.g. nitrate, chloride, sulfate, and carbonate) with phosphate. The concentrations of individual anions were in the range of 0.5-5 mmol/L. AMCR (0.1 g) were added to a set of 100 ml Erlenmeyer flasks containing 25 mL of solutions with co-existed anions. After stirring for 60 min, the residual nitrate was determined.

3. Results and discussions

3.1. Characteristics of all magnetic samples

3.1.1. VSM curves of all magnetic samples

The magnetic property of the magnetic sample were analyzed by VSM at room temperature and the results were shown in Fig. 2A. The zero coercivity and reversible hysteresis behavior were observed in the VSM curve of ACMR; this was consistent with the previous studies. The result indicated that this magnetic biomaterial was superparamagnetic with low hysteresis loss. The saturated magnetization value of ACMR was measured to be 7.87 emu/g; this was similar to the reported magnetic biosorbents with range of 6.33-8.89 emu/g [11, 20, 21]. With such high saturated magnetization, the ACMR could be easily recovered from the aqueous solution (collected less than 1 min) by applying an external magnetic field.

The magnetic property of the spent ACMR after the adsorption of phosphate was

also determined and its saturated magnetization value was measured to be 6.77 emu/g. Although the magnetic property of ACMR was weakened after the adsorption process, the spent ACMR still presented a high saturated magnetization, which could be separated easily from treated solution by an external magnetic field.

The magnetic property of the regenerated ACMR was also recovered after the 4 cycles of brine regeneration process. The saturated magnetization of the regenerated sample was measured to be 7.49 emu/g; this was very close to the clean ACMR but higher than that of spent sample. This result indicated that effect of brine desorption process on magnetic property of ACMR was negligible. As a result, ACMR could be reused without significant loss in magnetization.

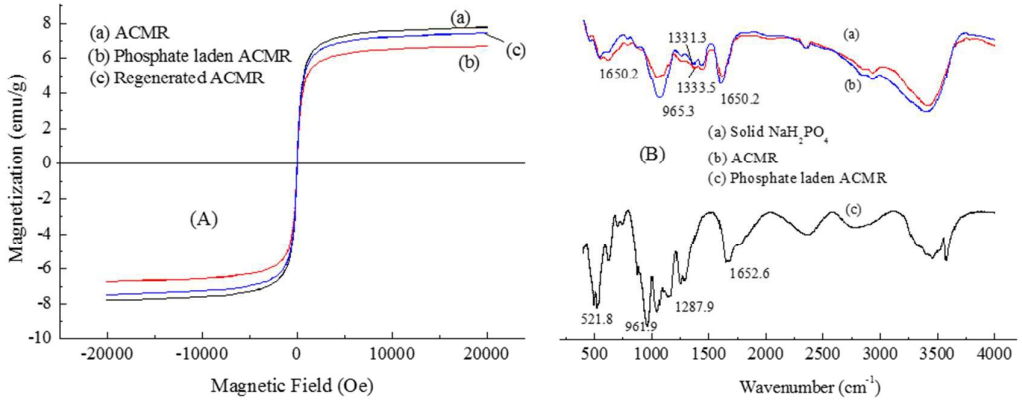

Fig. 2. Magnetization curves of all ACMR samples (A); FT-IR spectra of all ACMR samples (B)

The powder XRD patterns of ACMR and Fe_3O_4 are shown in Fig. S1A. For XRD pattern of Fe_3O_4 five characteristic peaks at 30.1°, 35.4°, 43.0°, 56.9° and 62.5° were corresponding to the (220), (311), (400), (511) and (440) crystal planes of a pure Fe_3O_4 with a spinal structure [15] .The chemical reaction of Fe3O4 formation can be written as:

$$Fe^{2+} + 2Fe^{3+} + 8OH^- \rightarrow Fe_3O_4 + 4H_2O$$

Compared with the XRD pattern of Fe_3O_4 ,we can see that the Fe_3O_4 crystal has been successfully grown onto the virgin reed template. In addition, it was observed that diffraction peaks at $2\theta = 15.5^o$ and 22.6° assigned to crystalline cellulose can be found for ACMR [15].

3.1.2. FT-IR spectra of clean ACMR, phosphate laden ACMR

FT-IR spectra of clean ACMR, phosphate laden ACMR and solid phosphate were shown in Fig. 2B. The absorption bands at 588, 610, 630 and 790 cm^{-1} are the characteristics of the Fe–O vibrations (Fe_3O_4) in clean ACMR after co-precipitation [16, 22, 23]. The absorption peak at around 1169.4 cm^{-1} for ACMR indicated the

existence of the C–O bond in the carboxylic groups or the O–C stretching vibrations in the ester structures [2, 19]. After amine cross-linking reactions, the bands at 1540.6 and 1331.3 cm^{-1} were observed in the spectra of clean ACMR, corresponding to N–H, C–N bending vibration in ACMR. These observations provide evidence that amine groups and Fe_3O_4 nanoparticles have been successfully introduced onto the surface of virgin reed, forming the amine functionalized magnetic reed.

The specific peaks of solid Na_2HPO_4 were observed at 521.8, 961.9, 1287.9 and 1652.6 cm^{-1}. It was obvious that these peaks were also overlapped with the bands of phosphate-loaded ACMR and the specific bands (1100-1250 cm^{-1} and 1650 cm^{-1}) in phosphate-loaded ACMR were greatly enhanced. In addition, C–N bond (1331.3 cm^{-1}) in ACMR was shifted to 1333.5 cm^{-1} after the adsorption of phosphate. These results indicated that phosphate was adsorbed onto the surface of ACMR by interactions between amine groups and phosphate.

3.1.3. SEM and TEM of ACMR

SEM images of the ACMR at different magnification were shown in Fig. 3. It was obvious that the ACMR was based on lignocellulosic structures with homogeneous and relatively smooth surface (Fig. 3a). In addition, some intricate channels were formed at the margin of the lignocellulosic structures (Fig. 3b); this increased the surface areas of ACMR (34.3 m^2/g) as compared with 4.8 m^2/g of virgin reed. BET surface area of ACMR was increased almost 7 times after the Fe_3O_4 in-situ co-precipitation and amine functionalization processes. As a result, ACMR could provide a higher contact area and more sufficient active sites for phosphate removal.

The typical TEM images of ACMR was shown in Fig. 3 (c and d). It was evident that TEM image of ACMR was of irregular shape with Fe_3O_4 nanoparticles embedded in virgin reed. The average particle diameter of present Fe_3O_4 was approximately 10.4 nm; this corresponded well to the previous study [15, 16, 24, 25]. As a result, a large number of Fe_3O_4 had been introduced onto the skeleton of reed, which made the magnetic reed easily be separated from aqueous solution by a magnetic process.

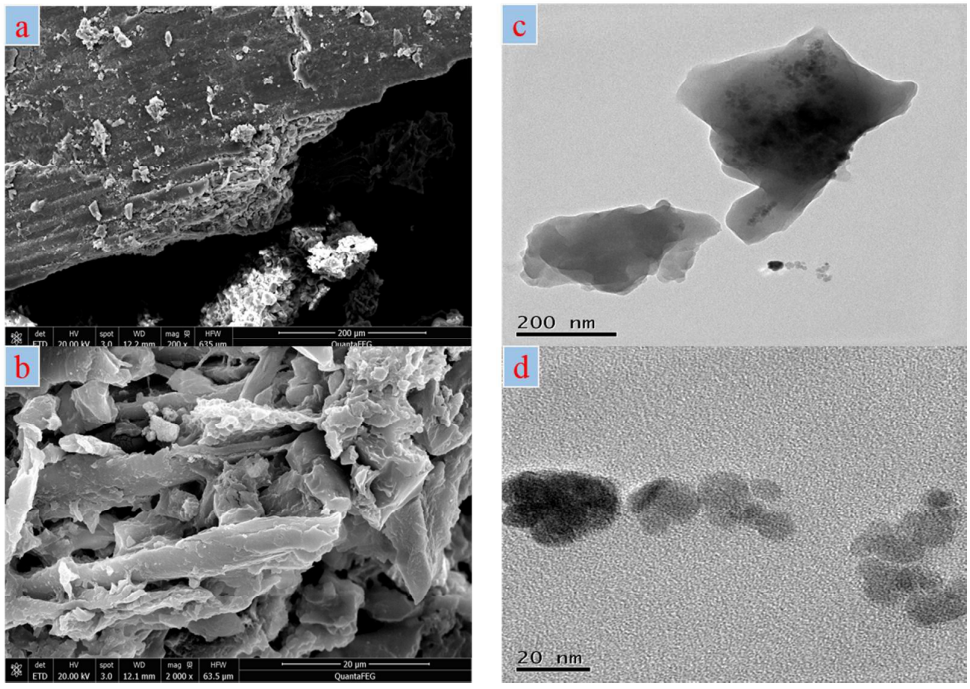

Fig. 3 SEM images of ACMR at different magnification (a) ×200, (b) ×2000; TEM of ACMR (c) 200 nm, (d) 20 nm

3.1.4. XPS of clean ACMR, phosphate laden ACMR and regenerated ACMR

The XPS wide scan spectra of clean ACMR, phosphate laden ACMR as well as regenerated ACMR were shown in Fig. 4. The binding energies at around 284, and 532 eV corresponded to the C1s, and O1s, which were the basic elements in all ACMR samples. Their atomic ratios were constant with 66.7-68.6% for C 1s and 16.7-18.2% for O 1s.

The Cl 2p (196.6 eV) in clean ACMR was derived from epichlorohydrin, which corresponded to the adsorption sites for phosphate. This binding energy almost disappeared after the adsorption of phosphate; it was replaced by the new binding energy at 133.4 eV, which was assigned to the adsorbed phosphate on surface of ACMR. After the brine regeneration, the atomic ratio of P significantly decreased from 1.61% to 0.27% with the increase of Cl atomic ratio from 0.45 to 4.04%. This indicated that brine regeneration process was effective to desorb the laden phosphate from ACMR.

The typical peaks for Fe in XPS analysis were at 711, and 729 eV, representing binding energies of Fe 2p. The peaks at 710.1 eV related to Fe(II) and the shoulder peak at 724.3 eV assigned to Fe(III) suggested the co-existence of Fe(III) and Fe(II) of Fe_3O_4 in all ACMR samples. After four cycles of adsorption-desorption processes,

the atomic ratio of Fe in regenerated ACMR was about 0.41%, which was a bit lower as compared with that of clean sample (0.46%); this indicated a small loss of Fe_3O_4 on surface of ACMR during adsorption-desorption cycles.

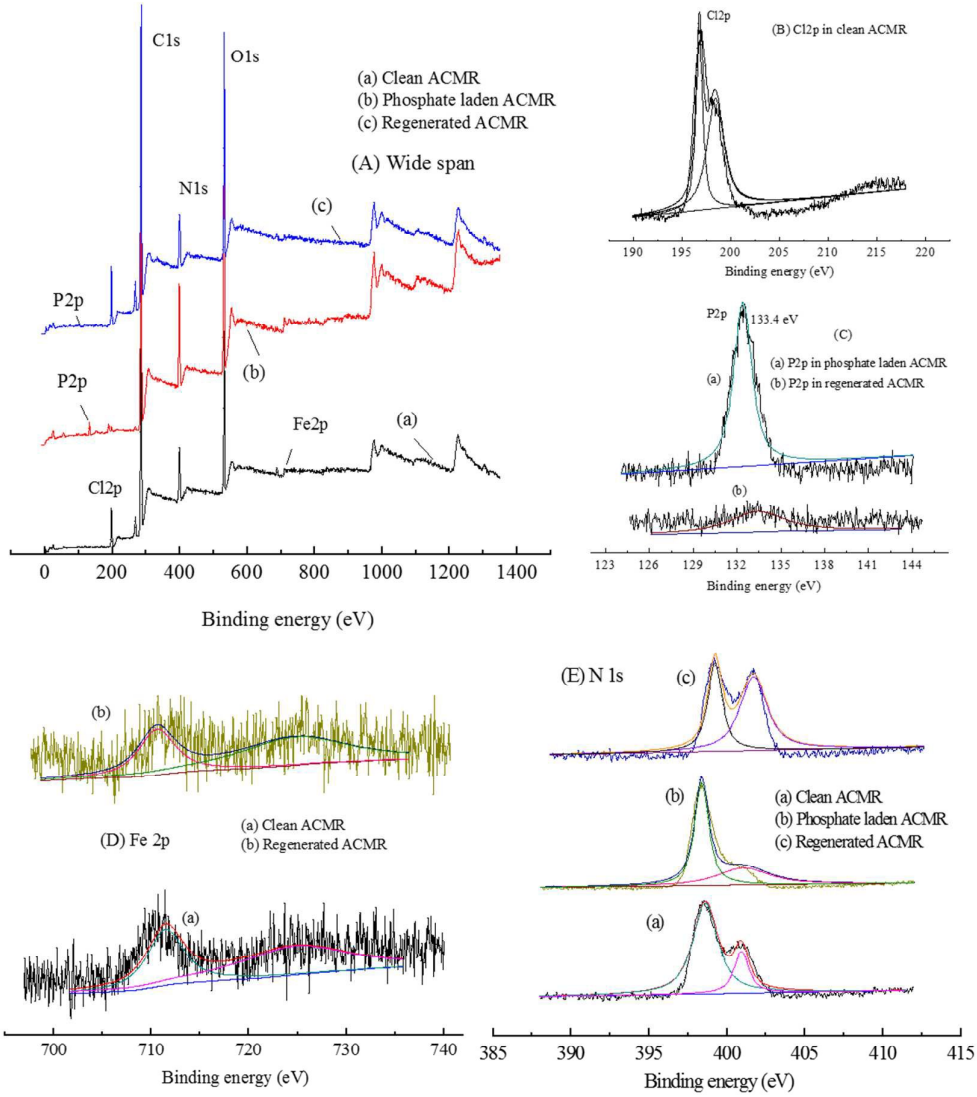

Fig.4 XPS of Clean ACMR and phosphate laden ACMR (A) wide scan (0-1400 eV); (B)Cl 2p (190-217 eV); (C)P 2p (125-145 eV); (D) Fe 2p (695-740 eV); (E) N 1s (387-412 eV)

The narrow scan of N 1s at 397-415 eV was shown in Fig. 4E. The one with lower binding energy (~399.4 eV) could be interpreted as N in amide[26]. The binding energy value at higher N state (401.4 eV) was assigned to the N^+ in quaternary nitrogen N1s[26]. After phosphate adsorption, N 1s of N^+ in quaternary nitrogen was weakened and shifted to 401.8 eV. This peak was recovered after the brine desorption process with binding energy at 401.3 eV. In contrast, the N 1s at ~399.4 eV was

almost constant. These results indicated that the adsorption of phosphate was mainly based on the N^+ in quaternary nitrogen. The atomic ratio of N in regenerated ACMR was about 10.75%, which was a slight lower than that in clean ACMR (11.05%); this indicated an extent of destruction of amine groups during several cycles of adsorption-desorption processes.

3.2. Adsorption tests

3.2.1. Adsorption of phosphate by ACMR as a function of pH

The adsorption of phosphate onto ACMR as a function of pH are shown in Fig. 5. Equilibrium pH values were examined after the uptake of phosphate by ACMR at different initial pHs. A significant decrease in the equilibrium pH is observed as compared to the initial data with range of 4.0-11.0. This could be partially due to the weakly acidic hydroxyl and carboxyl inherently in structure of ACMR, which would decrease the pH conditions in adsorption system.

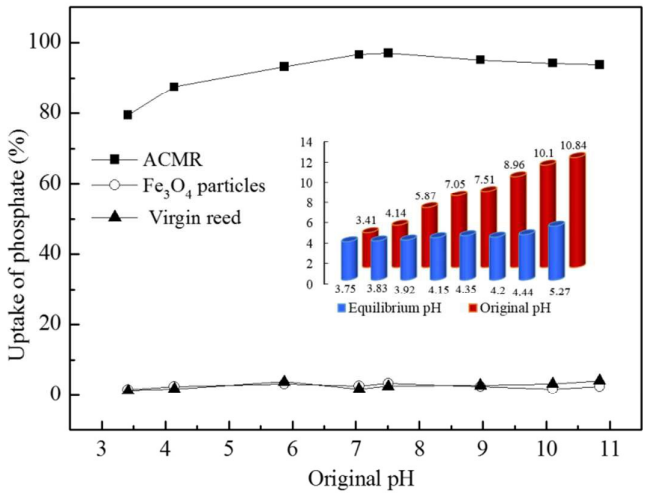

Fig. 5 Adsorption of phosphate by ACMR as a function of pH (phosphate concentration: 40 mg P/L, contact time: 60 min, ACMR dosage: 4 g/L, temperatures: 20°C)

Both Fe_3O_4 particles and virgin reed were used for uptake of phosphate, but their uptake capacities were lower than 4% at all pH conditions (Fig. 5). Results shown in Fig. 5 also indicated that uptake of phosphate by ACMR was increased from 78.7% to 97.1% with an increased pH from 3.1 to 7.5; thereafter the uptake was slightly decreased to 94.8% with the pH increased from 7.5 to 10.8. Based on the adsorption data, it is apparent that the phosphate adsorption capacities are reduced with pHs at strong acid and strong base conditions.

When the pH was lower than 4.0, the species of phosphate ions in the system mainly exist in the form of H_3PO_4 and $H_2PO_4^-$. The lowering of pH caused phosphate

to be protonated and the increased phosphoric acid will interfere with the adsorption of phosphate by ACMR. When the pH increased beyond 10.0, the OH^- will increase significantly, and the excess OH^- in the system would compete with phosphate ions for adsorption sites on surface of ACMR. In addition, the surface of ACMR will be negatively charged at higher pHs [27]. Both these factors weakened the interactions between the negatively charged phosphate ions and positively charged ACMR, etc. resulting in a decreased uptake of phosphate at higher pH conditions.

3.2.2. Adsorption isotherms

The adsorption isotherms of phosphate by ACMR at different temperature (20, 35 and 45 °C) were determined over a wide range of phosphate concentrations from 25 to 500 mg/L. Its adsorption isotherms curves were shown in Fig. 6a. The experimental adsorption capacities (Q_{exp}) at 20, 35 and 45 °C was evaluated to be 36.9, 33.2 and 31.6 mg/g. The Q_{exp} decreased with the increase of temperature; this indicated that the phosphate adsorption by ACMR was an exothermic process.

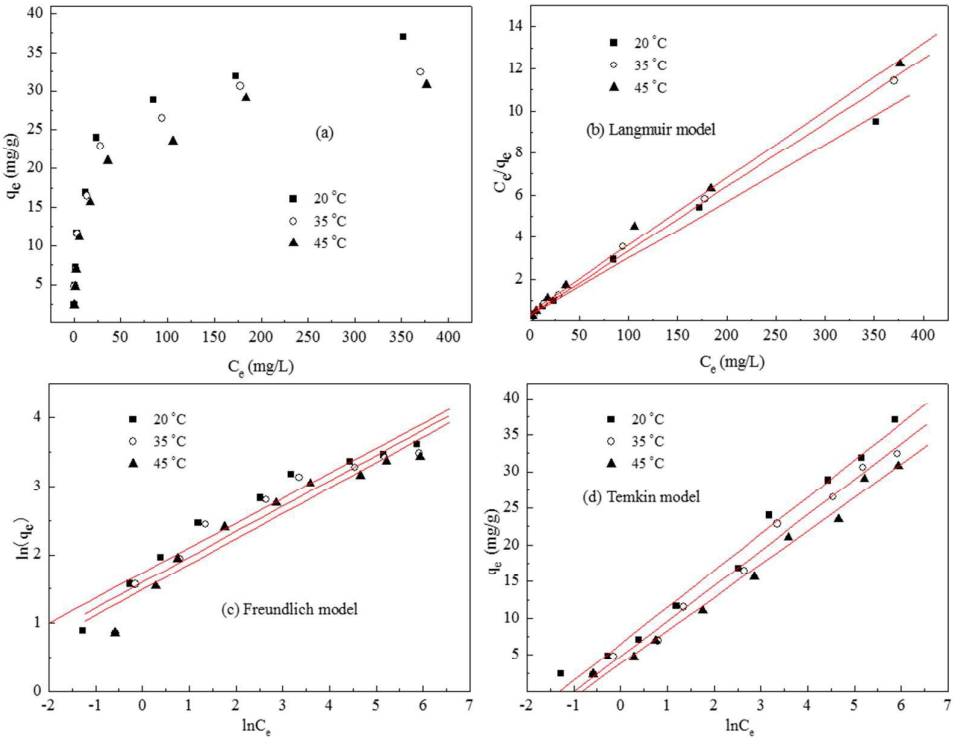

Fig. 6 Adsorption isotherms of phosphate by ACMR at different temperature (20, 35 and 45 °C)

All equilibrium results were fit with the Langmuir, Freundlich, and Temkin models followed as[28-31]:

Langmuir model: $$\frac{1}{q_e} = \frac{1}{Q_{\max}} + \frac{1}{bQ_{\max}} \frac{1}{C_e} \quad (1)$$

Freundlich model: $\ln q_e = \ln K_F + \frac{1}{n}\ln C_e$ (2)

Temkin equation: q_e=B ln (AC_e) (3)

Where Q_{max} is the maximum adsorption capacity (mg/g); b is Langmuir constant (mg^{-1}).K_F is the Freundlich constant (mg/g)/(mg/l), and n is a dimensionless exponent between 0 and 1 relating to the degree of surface heterogeneity. A and B are Temkin isotherm constants.

The fit of the three isotherms (Langmuir, Freundlich, and Temkin models) was shown in Fig. 6b-d and their parameters were summarized in Table 1. The experimental data were fit well by the Langmuir with correlation coefficient R^2between 0.994-0.998. Since the Langmuir equation assumes that the surface is homogenous, as a result, the adsorption of phosphate by ACMR was based on the homogenous distribution of adsorption sites on surface of the magnetic biocomposite. The calculated Q_{max} from Langmuir model were about 37.0, 33.0 and 31.4 mg/g at 20, 35 and 45 °C; this was very close to the experimental data. The phosphate capacities of different magnetic composites was evaluated by Yan et al [32], and they found that uptake of phosphate by reported Fe_3O_4 composites were in range of 2.0-37.0 mg/g. As a result, the magnetic biocomposite prepared in this work has shown comparable phosphate uptake capacity by contrast with most reported work.

Temkin isotherm contains a factor that explicitly takes into account adsorbing species-adsorbate interactions[31, 33]. This model assumes the following: (i) the adsorption is characterized by a uniform distribution of binding energies, up to some maximum binding energy, and that (ii) the heat of adsorption of all molecules in the layer decreases linearly with coverage due to adsorbent–adsorbate interactions. The correlation coefficients R^2 obtained from Temkin model (0.987-0.991) were relatively higher than those of Freundlich model. As a result, the adsorption of phosphate onto ACMR could also be characterized by a uniform distribution of binding energies and potential interactions between the phosphate and homogenous surface of ACMR.

Table 1 Langmuir, Freundlich, and Temkin constants for adsorption of phosphate by ACMR

Temperature	Langmuir			Freundlich			Temkin		
(°C)	Q_{max} (mg/g)	b	R^2	K_F (mg/g)/(mg/l)	n	R^2	A	B	R^2
20	37.0	0.0878	0.994	5.62	2.74	0.938	3.65	5.01	0.987
35	33.0	0.0925	0.998	4.93	2.69	0.906	2.72	4.82	0.990
45	31.4	0.0720	0.995	4.43	2.68	0.930	2.28	4.55	0.991

3.2.3. Adsorption kinetics

Adsorption kinetics, demonstrating the solute uptake rate, is one of the most important characteristics which represents essential information on the reaction pathways, and therefore, determines their potential applications.

Results shown in Fig. 7 indicated that the amount of adsorbed phosphate increased with time *t* and the adsorption reached an equilibrium state within 10-15 min. There was two adsorption stages before the equilibrium. It was obvious that about 70% of phosphate was removed within 1~5 min in stage 1; this represented a rapid adsorption rate partially due to the instantaneous monolayer adsorption on surface of ACMR. The rapid adsorption process was then followed by a gradually reduced adsorption rate prior to reaching equilibrium (Stage 2).

To analyze the adsorption rate of phosphate onto MWS, the pseudo first-order equation, pseudo second-order equation and intra-particle diffusion equation were evaluated based on the experimental data [14, 34, 35].

(1) Pseudo first-order model

A kinetic model for adsorption analysis is the pseudo first-order rate expressed in the form:

$$\ln(q_e - q_t) = \ln q_e - k_1 t \quad (4)$$

Where q_e and q_t are the amounts of phosphate adsorbed per gram ACMR at equilibrium and time t (mg/g); k_1 is the rate constant of pseudo first-order (min^{-1}).

(2) pseudo second-order model

The pseudo second-order kinetic rate equation is given as follows:

$$\frac{t}{q_t} = \frac{1}{k_2 q_e^{\ 2}} + \frac{t}{q_e} \quad (5)$$

where k_2 is the equilibrium rate constant of pseudo second-order (g/(mg min))

(3) Intra-particle diffusion model

The intra-particle diffusion model was proposed to identify the diffusion mechanism. If the plot of uptake, *qt*, versus square root of time, $t^{1/2}$ passes through the origin, the intra-particle diffusion will be the sole rate-limiting process. The initial rate of intra-particle equation is as follows:

$$q_t = k_p t^{0.5} \quad (6)$$

Where k_p is the intra-particle rate constant ($g \cdot mg^{-1} \cdot min^{-0.5}$), and the intra-particle rate constant k_p is a function of equilibrium concentration in solid phase q_e and intra-particle diffusivity *D* according to the equation expressed as:

$$k_p = \frac{6q_e}{R}\sqrt{\frac{D}{\pi}} \quad (7)$$

Where R is the particle radius and D is intra-particle diffusivity.

Kinetic parameters at different phosphate concentrations were evaluated from the Fig. 7 b-d and all results were given in Table 2. The correlation coefficients (R^2) obtained from the pseudo first-order kinetic model were only 0.699-0.947, which were significantly lower than those of the correlation coefficients (R^2) from pseudo second-order kinetic model (>0.999). And also, the calculated q_{e2} values (2.45-9.12 mg/g) obtained at different phosphate concentrations (10-40 mg/g) agree well with experimental $q_{e,exp}$ values (2.42-9.05 mg/g).

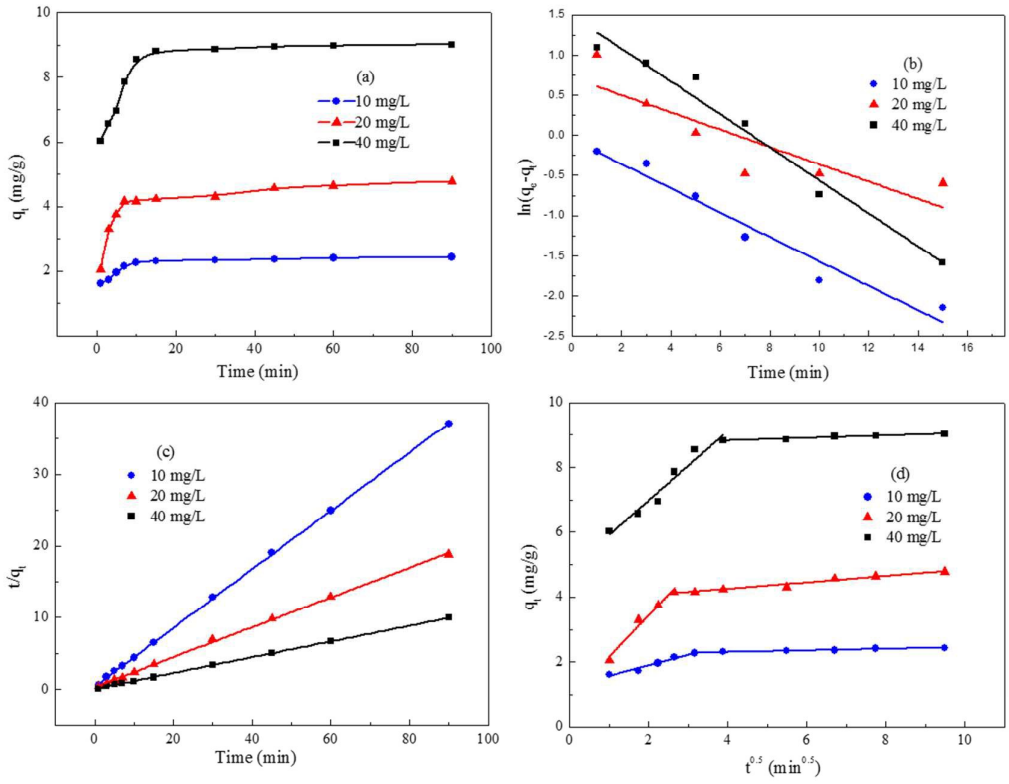

Fig. 7 (a) Adsorption kinetic of phosphate onto ACMR and (b) its fit with Pseudo first-order model; (c)Pseudo second-order model; (d) Intra-particle diffusion model

Based on the results from Fig. 7d, it was obvious that the plots of qt versus $t^{1/2}$ exhibited an initial linear portion followed by a plateau after 10-15 min. The initial curved portion of the plots corresponded to the boundary layer adsorption in the first adsorption stage and the linear portion to intra-particle diffusion, with the plateau corresponding to equilibrium. In addition, the plots did not pass through the origin. This indicated that intra-particle diffusion was not the only rate-limiting step; other

kinetic processes were also simultaneously involved in the adsorption, which both contributed to the adsorption mechanisms for phosphate onto ACMR.

Table 2 Kinetic parameters for adsorption rate expressions

C_0 (mg/L)	q_{eexp}[a] (mg/g)	pseudo first-order			pseudo second-order			intra-particle diffusion	
		k_1 min^{-1}	q_{e1}[b] mg/g	R^2	k_2 g/(mg min)	q_{e2}[b] mg/g	R^2	k_p mg/(g min)	R^2
10	2.42	0.155	0.95	0.943	0.391	2.45	1	0.327	0.951
20	4.75	0.108	2.04	0.699	0.118	4.81	0.999	1.27	0.962
40	9.05	0.201	4.44	0.947	0.119	9.12	1	1.07	0.941

[a] $q_{e,exp}$ is experimental values; [b] q_{e1}, [b] q_{e2} are calculated values

3.2.4. Regeneration cycles

Desorption of laden phosphate from ACMR was conducted by using 0.1 mol/L of HCl, NaCl and NaOH solutions. After four cycles of adsorption-desorption process, the recovery of phosphate was decreased from 30.2 mg/g to 28.5, 27.1 and 25.5 mg/g with HCl, NaCl and NaOH as eluents, respectively (Fig. 8a). HCl and NaCl seemed to be more effective to regenerate the spent ACMR as compared with that of NaOH. This led to the conclusion that the adsorption of phosphate onto ACMR was reversible. No significant loss in adsorption capacity after four adsorption-desorption cycles (HCl and NaCl as eluents) demonstrated that the magnetic biocomposite was very suitable for the design of a continuous adsorption process. In addition, a higher concentration of eluent seemed to be optimal for desorption of laden phosphate from ACMR (Fig. 8b).

A decrease in adsorbed amount of phosphate may be, in part, due to loss of quaternary ammonium functional groups from the surface of ACMR during the brine desorption processes; this was validated by the XPS results of N1s. Another possibility of reduced adsorption was that the laden phosphate ions were continuously trapped within the inner surface of the channels or pores in ACMR, resulting in the small decrease in adsorption sites that were available throughout the adsorption–desorption cycles.

The atomic ratio of Fe in all regenerated ACMR samples (regenerated by HCl solution) was evaluated based on the XPS analysis (Fig. 8c). A gradual decrease in regenerated ACMR samples was observed as the adsorption-desorption cycles was carried out. The atomic ratio of Fe was almost reduced by 20% after 4 cycles of adsorption-desorption. However, the saturated magnetization value of regenerated

ACMR was decreased only lower than 5% (Fig. 2); this indicated that the loss of Fe during desorption process was mainly assigned to the Fe_2O_3 or other Fe formations, not to the Fe_3O_4 nano-particles in ACMR.

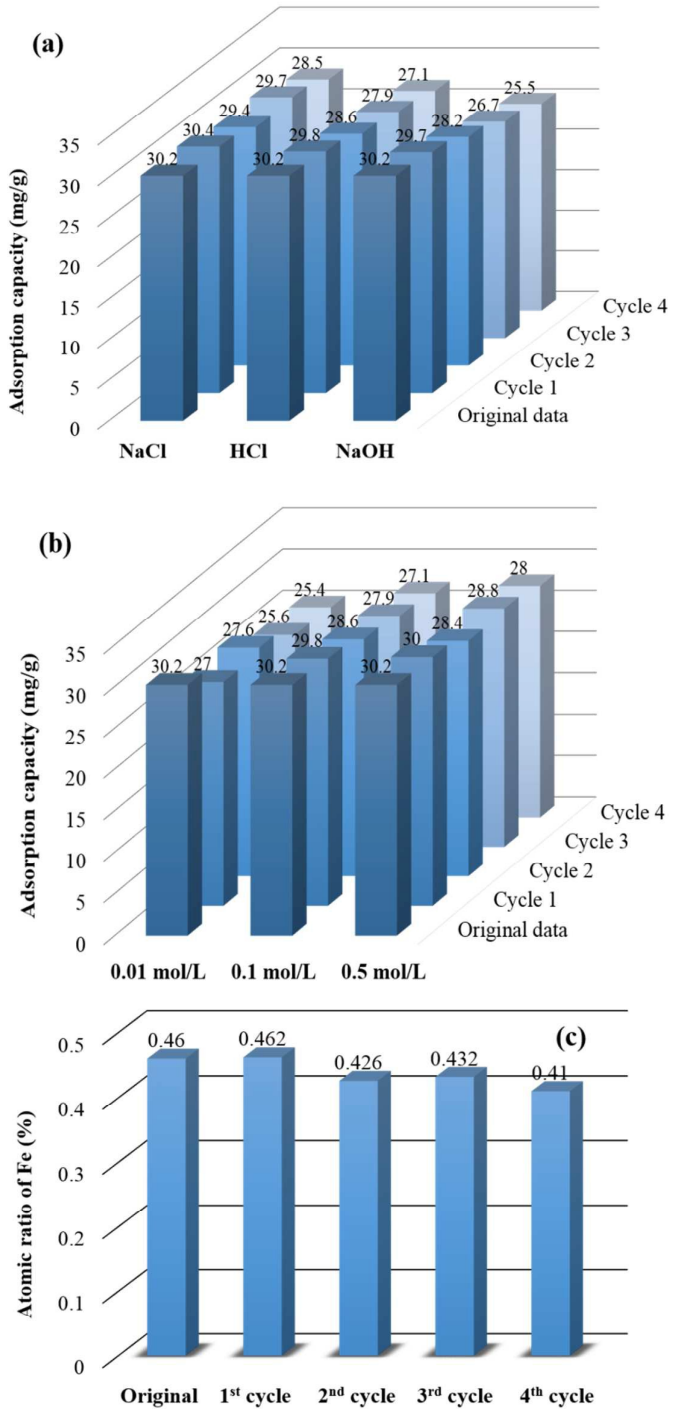

Fig. 8 (a) Adsorption-desorption results by using 0.1 mol/L of HCl, NaCl and NaOH as eluents; (b) Adsorption-desorption results by using 0.01 mol/L, 0.1 mol/L and 0.5 mol/L of HCl as eluents; (c) Atomic ratio of Fe (%) change in regenerated ACMR during adsorption-desorption cycles (0.1 mol/L of HCl solution as eluent)

3.2.5. Competitive adsorption

In the natural water environment, the phosphate ions are often co-existed with a series of other anions, such as nitrate, chloride, sulfate, and carbonate. The co-existing anions could compete with phosphate ions for the adsorption sites on surface of ACMR and decreasedits uptake for phosphate. Results indicated that the effect ofcompetitive ions was the greatest for NO_3^-, followed by SO_4^{2-} and Cl^- while therewas no effect of carbonate (Fig. 9). This result corresponded well to the reported work of Cho [36].The phosphate uptake capacity was reduced by 45% in the presence of 5 mmol/L NO_3^-, by 32% in the presence of 5 mmol/L SO_4^{2-}, and by 23% in the presence of Cl^-. Results in Fig. 9 also showed that the uptake of phosphate even increased slightly in the presence of 1 and 2 mmol/L carbonate ions. This might be partially assigned to the equilibrated pH of the adsorption systemdue to the co-existed carbonate anions, which was optimal for phosphate adsorption.

As discussed in this work, the adsorption of phosphate by ACMR was based on ions exchange on quaternary ammonium groups. As a result, the inhibition effect was more significant for anions with greater tendency to undergo ion exchange reaction (e.g. sulfate, nitrate and chloride) with quaternary ammonium groups on ACMR.

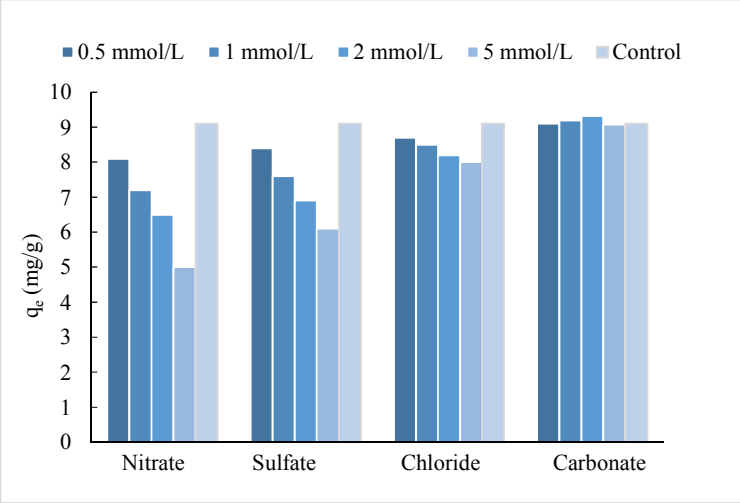

Fig. 9 Effect of co-existing anions on the uptake of phosphate by ACMR

Conclusions

ACMR was prepared by Fe_3O_4 in-situ co-precipitation and amine functionalization methods by using virgin reed as starting material. The characteristics of virgin, spent and regenerated samples were measured by FTIR, TEM, SEM, VSM and XPS. Results from FTIR and XPS analysis indicated that phosphate was adsorbed onto the surface of ACMR by interactions between amine groups and phosphate. The adsorption of phosphate onto ACMR could also be characterized by a uniform

distribution of binding energies and potential interactions between the phosphate and homogenous surface of ACMR. Effect of competitive ions was the greatest for NO_3^-, followed by SO_4^{2-} and Cl^- while there was no effect of carbonate. In addition, no significant loss in adsorption capacity during four adsorption-desorptioncycles (HCl and NaCl as eluents) demonstrated that the magnetic biocomposite was very suitablefor the design of a continuous adsorption process.

Acknowledgments

The research was supported by the National Natural Science Foundation of China (51178252, 51508307), China Postdoctoral Science Foundation funded project (2014M560556, 2015T80721). This work was also supported by grants from Tai Shan Scholar Foundation.

References

[1] Z. Ren, X. Xu, B. Gao, Q. Yue, W. Song, Integration of adsorption and direct bio-reduction of perchlorate on surface of cotton stalk based resin, J. Colloid Inter. Sci., 459 (2015) 127-135.

[2] X. Xu, B. Gao, W. Wang, Q. Yue, Y. Wang, S. Ni, Adsorption of phosphate from aqueous solutions onto modified wheat residue: Characteristics, kinetic and column studies, Colloids Surfaces B: Biointerfaces, 70 (2009) 46-52.

[3] X. Xu, B.-Y. Gao, X. Tan, Q.-Y. Yue, Q.-Q. Zhong, Q. Li, Characteristics of amine-crosslinked wheat straw and its adsorption mechanisms for phosphate and chromium (VI) removal from aqueous solution, Carbohydr. Polym., 84 (2011) 1054-1060.

[4] J. Lalley, C. Han, X. Li, D.D. Dionysiou, M.N. Nadagouda, Phosphate adsorption using modified iron oxide-based sorbents in lake water: Kinetics, equilibrium, and column tests, Chem. Eng. J., 284 (2016) 1386-1396.

[5] Y. Yan, X. Sun, F. Ma, J. Li, J. Shen, W. Han, X. Liu, L. Wang, Removal of phosphate from wastewater using alkaline residue, J. Environ. Sci., 26 (2014) 970-980.

[6] T.A.H. Nguyen, H.H. Ngo, W.S. Guo, T.Q. Pham, F.M. Li, T.V. Nguyen, X.T. Bui, Adsorption of phosphate from aqueous solutions and sewage using zirconium loaded okara (ZLO): Fixed-bed column study, Sci.Total Environ., 523 (2015) 40-49.

[7] T.A.H. Nguyen, H.H. Ngo, W.S. Guo, J. Zhang, S. Liang, D.J. Lee, P.D. Nguyen, X.T. Bui, Modification of agricultural waste/by-products for enhanced phosphate removal and recovery: Potential and obstacles, Bioresour. Technol., 169 (2014) 750-762.

[8] M.R. Awual, M.A. Shenashen, A. Jyo, H. Shiwaku, T. Yaita, Preparing of novel fibrous ligand exchange adsorbent for rapid column-mode trace phosphate removal from water, J. Ind. Eng. Chem., 20 (2014) 2840-2847.

[9] W. Wang, J. Zhou, D. Wei, H. Wan, S. Zheng, Z. Xu, D. Zhu, ZrO2-functionalized magnetic mesoporous SiO2 as effective phosphate adsorbent, J. Colloid Inter. Sci., 407 (2013) 442-449.

[10] S. Lata, S.R. Samadder, Removal of arsenic from water using nano adsorbents and challenges: A review, J. Environ. Manage., 166 (2016) 387-406.

[11] D. Mehta, S. Mazumdar, S.K. Singh, Magnetic adsorbents for the treatment of water/wastewater—A review, J. Water Process Eng., 7 (2015) 244-265.

[12] V.K. Sharma, T.J. McDonald, H. Kim, V.K. Garg, Magnetic graphene–carbon nanotube iron nanocomposites as adsorbents and antibacterial agents for water purification, Adv. Colloid Inter. Sci., 225 (2015) 229-240.

[13] A.E. Chávez-Guajardo, J.C. Medina-Llamas, L. Maqueira, C.A.S. Andrade, K.G.B. Alves, C.P. de Melo, Efficient removal of Cr (VI) and Cu (II) ions from aqueous media by use of polypyrrole/maghemite and polyaniline/maghemite magnetic nanocomposites, Chem. Eng. J., 281 (2015) 826-836.

[14] X. Sun, L. Yang, Q. Li, J. Zhao, X. Li, X. Wang, H. Liu, Amino-functionalized magnetic cellulose nanocomposite as adsorbent for removal of Cr(VI): Synthesis and adsorption studies, Chem. Eng. J., 241 (2014) 175-183.

[15] W. Song, B. Gao, X. Xu, F. Wang, N. Xue, S. Sun, W. Song, R. Jia, Adsorption of nitrate from aqueous solution by magnetic amine-crosslinked biopolymer based corn stalk and its chemical regeneration property, J. hazard. mater., 304 (2016) 280-290.

[16] W. Song, B. Gao, T. Zhang, X. Xu, X. Huang, H. Yu, Q. Yue, High-capacity adsorption of dissolved hexavalent chromium using amine-functionalized magnetic corn stalk composites, Bioresour. technol., 190 (2015) 550-557.

[17] X. Xu, B. Gao, X. Huang, J. Ling, W. Song, Q. Yue, Physicochemical characteristics of epichlorohydrin, pyridine and trimethylamine functionalized cotton stalk and its adsorption/desorption properties for perchlorate, J. Colloid Inter. Sci., 440 (2015) 219-228.

[18] X. Xu, B. Gao, W. Wang, Q. Yue, Y. Wang, S. Ni, Effect of modifying agents on the preparation and properties of the new adsorbents from wheat straw, Bioresour.Technol., 101 (2010) 1477-1481.

[19] X. Xu, B. Gao, Q. Yue, Q. Zhong, Sorption of phosphate onto giant reed based adsorbent: FTIR, Raman spectrum analysis and dynamic sorption/desorption properties in filter bed, Bioresour. Technol., 102 (2011) 5278-5282.

[20] H. Ma, J.-B. Li, W.-W. Liu, M. Miao, B.-J. Cheng, S.-W. Zhu, Novel synthesis of a versatile magnetic adsorbent derived from corncob for dye removal, Bioresour.Technol., 190 (2015) 13-20.

[21] X.-F. Sun, B. Liu, Z. Jing, H. Wang, Preparation and adsorption property of xylan/poly(acrylic acid) magnetic nanocomposite hydrogel adsorbent, Carbohydr. Polym., 118

(2015) 16-23.
[22] N.M. Mahmoodi, Synthesis of core–shell magnetic adsorbent nanoparticle and selectivity analysis for binary system dye removal, J. Ind. Eng. Chem., 20 (2014) 2050-2058.
[23] F.-L. Mi, S.-J. Wu, Y.-C. Chen, Combination of carboxymethyl chitosan-coated magnetic nanoparticles and chitosan-citrate complex gel beads as a novel magnetic adsorbent, Carbohydr. Polym., 131 (2015) 255-263.
[24] N. Farzin Nejad, E. Shams, M.K. Amini, Synthesis of magnetic ordered mesoporous carbon (Fe-OMC) adsorbent and its evaluation for fuel desulfurization, J. Magn. Magn. Mater., 390 (2015) 1-7.
[25] C. Zhang, L. Chen, T.-J. Wang, C.-L. Su, Y. Jin, Synthesis and properties of a magnetic core–shell composite nano-adsorbent for fluoride removal from drinking water, Appl. Surf. Sci., 317 (2014) 552-559.
[26] R. Pietrzak, XPS study and physico-chemical properties of nitrogen-enriched microporous activated carbon from high volatile bituminous coal, Fuel, 88 (2009) 1871-1877.
[27] X. Xu, B.-Y. Gao, Q.-Y. Yue, Q.-Q. Zhong, Preparation and utilization of wheat straw bearing amine groups for the sorption of acid and reactive dyes from aqueous solutions, J. Hazard. Mater., 182 (2010) 1-9.
[28] L. Cui, L. Hu, X. Guo, Y. Zhang, Y. Wang, Q. Wei, B. Du, Kinetic, isotherm and thermodynamic investigations of Cu2 + adsorption onto magnesium hydroxyapatite/ferroferric oxide nano-composites with easy magnetic separation assistance, J. Mole. Liq., 198 (2014) 157-163.
[29] A.A. El-Bindary, M.A. Hussien, M.A. Diab, A.M. Eessa, Adsorption of Acid Yellow 99 by polyacrylonitrile/activated carbon composite: Kinetics, thermodynamics and isotherm studies, J. Mole. Liq., 197 (2014) 236-242.
[30] T.A. Khan, S.A. Chaudhry, I. Ali, Equilibrium uptake, isotherm and kinetic studies of Cd(II) adsorption onto iron oxide activated red mud from aqueous solution, J. Mole. Liq., 202 (2015) 165-175.
[31] A. Mittal, D. Jhare, J. Mittal, Adsorption of hazardous dye Eosin Yellow from aqueous solution onto waste material De-oiled Soya: Isotherm, kinetics and bulk removal, J. Mole. Liq., 179 (2013) 133-140.
[32] L.-g. Yan, K. Yang, R.-r. Shan, T. Yan, J. Wei, S.-j. Yu, H.-q. Yu, B. Du, Kinetic, isotherm and thermodynamic investigations of phosphate adsorption onto core–shell Fe3O4@LDHs composites with easy magnetic separation assistance, J. Colloid Inter. Sci., 448 (2015) 508-516.
[33] K.-Y.A. Lin, Y.-T. Liu, S.-Y. Chen, Adsorption of fluoride to UiO-66-NH2 in water: Stability, kinetic, isotherm and thermodynamic studies, J. Colloid Inter. Sci., 461 (2016) 79-87.

[34] J. Liu, R. Zhu, T. Xu, Y. Xu, F. Ge, Y. Xi, J. Zhu, H. He, Co-adsorption of phosphate and zinc(II) on the surface of ferrihydrite, Chemosphere, 144 (2016) 1148-1155.

[35] L. Song, J. Huo, X. Wang, F. Yang, J. He, C. Li, Phosphate adsorption by a Cu(II)-loaded polyethersulfone-type metal affinity membrane with the presence of coexistent ions, Chem. Eng. J., 284 (2016) 182-193.

[36] D.-W. Cho, C.-M. Chon, Y. Kim, B.-H. Jeon, F.W. Schwartz, E.-S. Lee, H. Song, Adsorption of nitrate and Cr(VI) by cationic polymer-modified granular activated carbon, Chem. Eng. J., 175 (2011) 298-305.